Available online at www.sciencedirect.com

ScienceDirect

Physics Procedia 55 (2014) 243 – 250

Physics Procedia

Eight International Conference on Material Science (CSM8-ISM5)

Electrochemical and Structural Characterization of Nickel Based Alloys Oxides

N.E Hakiki[1,*], J.L Bubendorff[2], C. Pirri[2], F. Mechehoud[1], A. Mehdaoui[2], M. Belhadji[3]

[1] *Laboratoire de Physique des Couches Minces et Matériaux pour l'Electronique (LPCM2E), Université d'Oran, BP 1524 El'Mnaouer Oran 31100, Algérie*
[2] *Institut de Science des Matériaux de Mulhouse (IS2M), LRC-CNRS 7228, Université de Haute Alsace, 4 rue des frères Lumière, 68093 Mulhouse Cedex, France*
[3] *Laboratoire de Chimie des Polymères (LCP), Université d'Oran, BP 1524 El'Mnaouer Oran 31100, Algérie*

Abstract

The electrochemical and structural characterization of thermally grown oxides formed on nickel based alloys (type Inconel 600 and 690) at 350°C and during different time was performed by impedance measurements and near field microscopy combining atomic force microscopy (AFM) and scanning Kelvin probe force microscopy (SKPFM). The impedance results allow discussing the influence of the oxidation time on the capacitance and the resistance of the oxide films. The results obtained by near field microscopy technique show that the film formed during low oxidation time has a small grain size and also a small surface roughness. The values of grain sizes determined in both cases along x- and y-axis are practically the same indicating a spherical shape of oxide grains and are slightly different between oxides formed on type inconel 600 and 690.

Peer-review under responsibility of the Organizing Committee of CSM8-ISM5

Key words: oxide, temperature, inconel, impedance, capacitance, scanning tunneling microscopy, atomic force microscopy, roughness.

1. Introduction

The nickel-based alloys are widely used in different chemical and nuclear domains. This concerns the equipment of chemical and nuclear power plants, especially steam generators in pressurized water reactors (PWR). Although some published works [1-3] have explored the properties of oxide layers of

* *Corresponding author. e-mail address: hakiki.noureddine@yahoo.fr or hakiki.noureddine@univ-oran.dz phone : (+213) 771 154 376*

Peer-review under responsibility of the Organizing Committee of CSM8-ISM5
doi:10.1016/j.phpro.2014.07.036

nickel-based alloys in different conditions and environments. Nevertheless, a detailed exploration of austenitic Ni-Cr-Fe alloys with high nickel content has received less attention than stainless steels. The important experimental works on these alloys are performed at high temperature, high pressure water, steam generators and simulation (SG) in the reactors pressurized water reactors (PWR) primary water, both in the dynamic flow conditions or in static autoclaves. It is most probable that the growth kinetics of the oxide film is closely related to the formation conditions, and hence the oxide films grown at different temperatures and/or different times have different layer properties among themselves. The nature of passive and oxide films formed on metals and alloys is the ultimate factor which controls their corrosion behaviour. Therefore, it is necessary to learn more about their structural and electronic properties to improve understanding of the corrosion processes and mechanisms which can be related to the morphologies, microstructures and chemical composition of the oxide films. A good knowledge of these corrosion processes and mechanisms allows us to find specific paths to prevent them from corrosion in high temperature and supercritical water. Consequently, a considerable number of investigations have been devoted to the study of the structural and electronic properties and chemical compositions of oxide and passive films, particularly on stainless steels and nickel base alloys. Experimental results reveal that, under certain conditions, the oxide films present gradients of chemical composition and can be constituted by regions of different semiconductivity [4-7]. It is now recognized that the surface oxide layer has a duplex structure formed by an inner Cr-rich layer and an outer layer consisting of well-defined octahedral Fe-rich crystals (stainless steels) or Ni-rich crystals (nickel alloys). However, the growth mechanism, the nature, composition and structure of the passive and thermally grown oxide films on Ni-based alloys remained largely unexplored. The electric properties of *passive* films and thermally grown oxides are often investigated by determining their capacitance *C*. This determination can be performed by in-situ measurements of the electrochemical impedance. The goal of the present work is to investigate structural and electric properties of thermally grown oxides on nickel-base alloys (Inconel 600 and 690), by examining the effect of oxidation time. These investigations have been performed by atomic force microscopy (AFM), scanning Kelvin probe force microscopy (SKPFM) and in-situ technique such as impedance measurements. Kelvin probe is a technique used to measure the surface potential (or Volta potential) of metals in vacuum or air. More than 20 years ago, Stratmann et al. [8] demonstrated a linear relationship between the Volta potential measured by a Kelvin probe and the corrosion potential of an electrode surface under a thin electrolyte layer.

2. Experiment

The Inconel type 600 (respectively 690) nickel based alloys used, has the following composition (wt%): Ni base, 16.30 Cr, 7.82 Fe, 0.65 Mn, 0.28 Si, 0.28 Ti, 0.033 C, 0.007 N, 0.007 P, 0.003 S (respectively Ni Base, 29.0 Cr, 10.0 Fe, 0.31 Si, 0.31 Ti, 0.30 Mn, 0.041 N, 0.015 C, 0.009 P, 0.001 S). For detailed information about the sample preparation and the used techniques, the reader is invited to consult reference [4-7]

3. Results and discussion

3.1. Open-circuit potential*:* The variation of rest potentials obtained for the thermally oxides formed at different oxidation times indicates that they are related to the formation conditions and reveal a continuous increase from -150 mV to 0 mV and from -250 mV to -30 mV for alloy 600 and 690, respectively, when the time of film formation is increased from 2h to 1176 h. Note that the difference potential of the rest potential exhibited by the two alloys is practically constant at about 100 mV and decreases at high oxidation time down to 40 mV. This behavior will be justified by the examination of capacitance and resistance results.

3.2. Impedance measurements*:* The capacitance and the resistance of the oxide layers can be investigated by impedance measurements where the real and imaginary parts of the electric impedance Z are determined as a function of the frequency f over a wide range 10^{-3} Hz –10^{5} Hz. Figure 1 shows typical Bode diagrams of the oxide layers formed on alloys 600 and 690. The Bode plots show typical capacitive-

like behaviour with one time constant and linear variation of the impedance modulus over a wide frequency range (5.10^{-3} Hz – 10^{3} Hz). They also show a slope smaller than unity, phase angle maxima smaller than 90° and a deviation which can be interpreted as a deviation of a double layer from ideal capacitance behaviour. The results obtained for thermally oxide layers formed at other oxidation conditions (not represented in this figure for sake of clarity) exhibit the same variation as those represented in the figure 1, indicating that the oxide layers exhibit the same qualitative behaviour in term of electrochemical impedance. The α slope values, obtained in the frequency range where the linear variation of Log Z versus Log F is obtained, varies between -0.86 and -0.95. They increase with increasing oxidation time. These variations indicate that more the modulus is less than unity more the frequency dispersion is important. Comparing the two investigated alloys, it can be deduced that the parameters values obtained in the first case deviate more from unity than those in the latter, indicating strong frequency dispersion where the oxide layers formed on alloy 600 are considered. Several reasons are evoked such as local inhomogeneities in the dielectric material, porosity, mass transport, relaxation effects, localized mid band gap states… The frequency dispersion of capacitance has been also reported in previous work on passive and oxide films [4-7].

In the case of passive and thermally grown oxides formed on stainless steels, the α values obtained in the first case (passive films) are higher (between -0.8 and -0.9) than those obtained for thermally oxide films (between -0.92 and -0.98) and so far to -1 indicating important frequency dispersion. These values, which decrease and tend to -1 with increasing formation potential, reveal that more important the frequency dispersion is more disordered the film is. It then presents high doping densities as discussed in the case of thermally oxide films. A more detailed investigation of electrochemical impedance and electric equivalent circuit models is taken into account and important results will soon be published in a next paper.

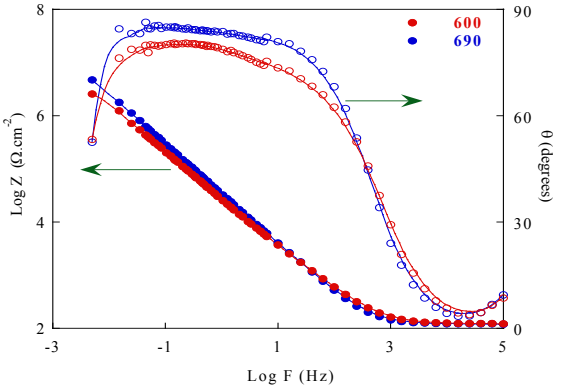

Figure 1: Bode plots for thermally grown oxides on alloys 600 and 690 at 350°C in air during 2h.

3.2.a. Capacitance and resistance results: The capacitance can be extracted from the imaginary part of the impedance. Despite this, the obtained capacitances remain correlated to the frequency. For this reason, the capacitance values that will be discussed below are extracted at high frequency (3160 Hz) in order to eliminate the contributions of surface states which are a slow phenomenon that influence the electrochemical response at low frequency.

Figure 2 shows the capacitance values obtained at the rest potential are presented at different oxidation times. It reveals the same qualitative variation for both oxide layers over a large domain of oxidation time. These variations are illustrated by a rapid decrease of the capacitance for the low oxidation times followed by a less pronounced decrease over the large domain. It is interesting to note that the capacitance values obtained on both oxide layers formed during 2 h at 350 °C are of the same order of magnitude as those obtained on thermally grown oxides formed at the same condition on AISI 304 stainless steel [4-6]. Note also that the capacitance values measured on the oxide layers formed on alloy 600 are weaker than that obtained on the alloy 690. Furthermore, the capacitance difference remains practically constant over the large investigated time domain. Assuming that there is a direct relationship between the capacitance and the open-circuit potential of the thermally grown oxide films, the results presented section 3.1 can be understood.

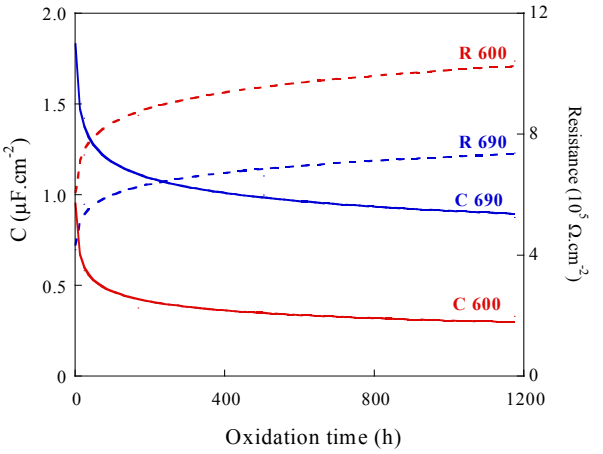

Figure 2: Influence of the oxidation time on the capacitance and the resistance of oxides formed on alloys 600 and 690 at 350°C.

In this figure, the resistance values obtained at the rest potential are presented in dashed lines at different oxidation times. It shows the same qualitative variation for both oxide layers over a large domain of oxidation time. These variations are illustrated by a rapid increase of the resistance for the low oxidation times followed by a less pronounced increase over the large domain. It is interesting to note that the qualitative variations of the resistances and the capacitances discussed above are inverted. It also remarked that the resistances measured on the oxide layers formed on alloy 600 are greater than that on the alloy 690. Also shown is that the difference of their resistances slowly increases with oxidation time. Finally, the values obtained in both cases, which vary between 0.4 $M\Omega.cm^{-2}$ and 1 $M\Omega.cm^{-2}$, are of the same order of magnitude as that obtained on 304 stainless steel [9, 10]. Note that the determination of these resistance results is complicated because in this study, the semicircles in the Nyquist diagram are too incomplete. In first approximation, this resistance can be determined at the lowest frequency. This method can be justified since the equivalent circuit model is composed by a pure resistance R_S, in series with a parallel combination of ideal resistance, R_P, and a constant phase elements, Q. The thickness of the space charge layer W_{sc} developed through the oxide films at the rest potentials can be deduced from the capacitance the capacitance by the relation $W_{sc}=\varepsilon\varepsilon_0/C$ where ε is the oxide dielectric constant, ε_0 is the vacuum permittivity and C the oxide layer capacitance. In the literature the permittivity of the oxide layers formed on stainless steels and nickel based alloys varies between 12 and 15.6, which is obviously a variation with the stoichiometry of the different oxides within the layer [4-6]. The value $\varepsilon=15.6$ taken in this work has often been used in previous works on nickel based alloy oxide layers [2-6]. According to section 3.1, all the rest potentials are higher than -0.5 V/SCE which corresponds to the flat band potential of the iron oxide [4-6]. We conclude than the space charge layers are developed in the iron oxide layer which behaves as an n-type semiconductor. The values of the space charge layer thicknesses W_{SC} obtained obey to a linear variation with oxidation time (in log-log representation) and show that the variation of W_{SC} in the case of the alloy 600 is more rapid than that of the alloy 690 oxide indicating a more important enlargement of the n-type iron oxide region in the alloy 600 grown oxides. Finally, since the thickness of the space charge layer is proportional to the oxide thickness, the results and discussion presented above can be used to obtain and discuss the oxide thickness evolution d_{ox} as a function of oxidation time. A more detailed analysis of the oxide growth mechanism and the modelling of the iron

oxide thickness as a function of oxidation time are taken into account in a recent work which will be published.

3.3. AFM and SKPFM results

3.3.a. Topography

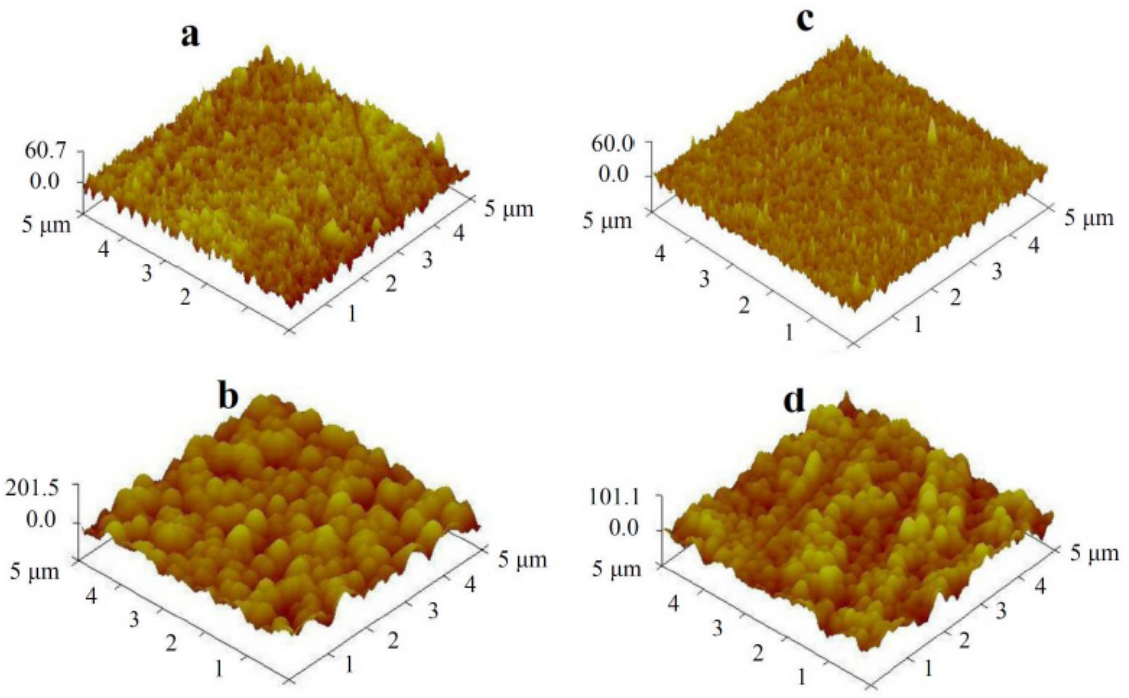

Figure 3: Atomic Force Microscopy images (three-dimensional view) of the samples oxidized in air at 350°C
during 1 day = 24 h (a : 600 c: 690) and 7 weeks = 1176 h (b :600 d: 690) .

Figure 1 shows AFM images (three-dimensional view) of the samples as a function of oxidation time. Fig. 1a and 1c respectively correspond to images of inconel 600 and 690 oxidized at the same time (t_{ox} = 24 h) whereas Fig. 1b and 1d show the images of the same samples at the highest oxidation time (t_{ox} = 7 weeks: 1176 h). Comparing images 1a and 1c with images 1b and 1d, we notice that the both grain size and surface roughness increases for both samples with increasing oxidation time but the roughness is more significant in image 1b than in image 1d. Secondly, it clearly appears that the grain size is more important in the case of oxidized alloy 600 than oxidized alloy 690. No important trenches are present indicating the good polishing of samples during experimental preparation. The observed grain-like structure corresponds to the oxide layer growth. To quantify these rough observations, we determine the surface roughness parameter (RMS) r as a function of the scan length of the surface area L and the grain size can be determined by using the RMS formula and the autocorrelation function for each oxidized

sample using the relation given in [11]. The values of s and r obtained as a function of oxidation time are given in table 1

Table 1: grain size (s) and roughness parameter (RMS) r at different oxidation time for oxide films formed on alloys 600 and 690.

Oxidation time	2h	24 h	168 h	567 h	1176 h
s_{600} (nm)	----	82	109	----	235
s_{690} (nm)	60	80	----	143	175
r_{600}(nm)	----	11.91	15.05	----	27.55
r_{690} (nm)	3.71	6.40	----	17.51	21.18

These values show that in both cases the grain size and the roughness r increase with increasing t_{ox} with the fact that the values determined for alloy 600 are not very different from those exhibited by alloy 690. These results are important because they indicate that the growth processes are similar in both alloys although the chromium concentrations are very different.

3.3.b Spectroscopy SKPFM

The surface potential images of the same region as for topographic AFM images (24h and 1176h) shown in figure 3, and acquired at 1V and 300 K, on oxidized alloys 600 and 690 are given in figure 4. This figure shows that the surface potential images are different from the topographic ones presented in figure 3. In figure 4, the low potential regions appear in dark while high potential regions appear in bright. This clearly shows that the Volta potential is independent of the topographic features. Figure 4 also shows that the observed contrast is related to a work function difference and not to topographic artifacts. So the potential contrast in figure 4 could correspond to a local chemical composition modification of the oxide film. The interpretation of SKPFM images is not easy in general, but possible in this case thanks to the previous knowledge of the oxide layer electronic structure. Indeed, previous results obtained by quantitative Auger analysis have shown that the layers are mainly constituted by an outer Fe_2O_3 iron oxide and an inner Cr_2O_3 chromium oxide in contact with the metallic substrate [4-6]. A localized disappearance of one of the two layers, and thus of the junction, makes corrosion possible. SKPFM images allow the localization of the areas where corrosion starts on a submicron scale. These areas are characterized by a higher Volta potential than the areas in which the p–n heterojunction is present (see discussion below). The interpretation of the measured Volta potential has been the subject of considerable discussions. Stratmann [8] studied the Volta potential of different metals covered with ultrathin electrolyte layers using the standard Kelvin probe, in which the probe did not touch the electrolyte layers.

The Volta potential was shown to have a linear correlation with the corrosion potential of the sample measured by a standard reference electrode positioned in the electrolyte layers. However, the Volta potential measured in air must be analyzed carefully because corrosion potential measured in a solution depends on the electrolyte composition. It was found that Cr and Ni richer oxide phases exhibit a higher Volta potential that Fe richer phases [12]. Nevertheless, no numerical values are given in the paper of Sathirachinda [12].

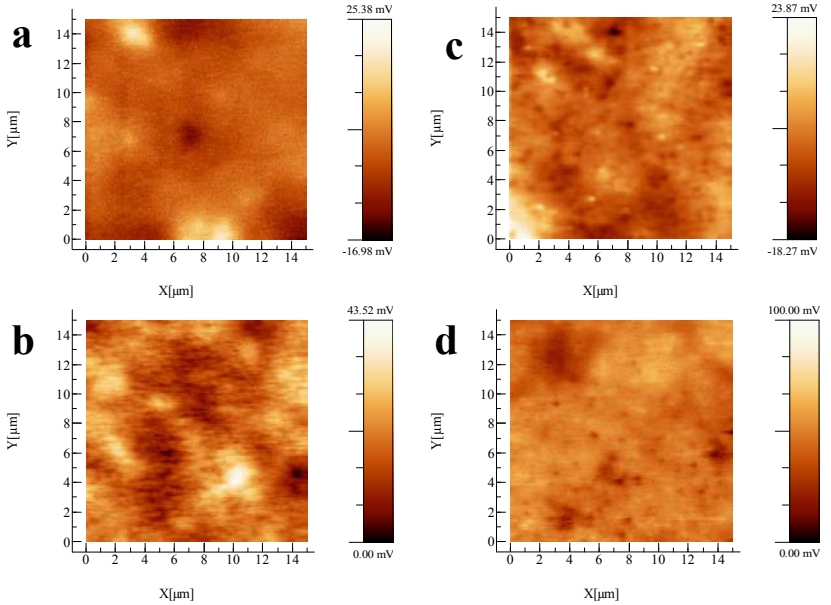

Figure 4: (SKPFM images of the samples oxidized in air at 350°C during 1 day = 24 h (a : 600 c: 690) and 7 weeks = 1176 h (b :600 d: 690)

To conclude this section, we show that at low t_{ox}, the double oxide layer structure could be absent from the surface locally at the micrometer scale. The surface oxide layer exhibits a local chromium enrichment which decreases the resistance toward pitting corrosion. These local corrosion sites are visualized in the SKPFM images. In contrast, at higher t_{ox}, the double oxide layer structure or heterojunction is complete and SKPFM images can be used to determine the oxide thickness (and thus the oxidation temperature) at which the protection is efficient

Conclusion

The combine impedance and AFM-SKPFM study of thermally grown oxides on alloys 600 and 690 at different oxidation times show that:

1- The capacitance of the space charge layer developed trough the oxides which behave as a semiconductors decreases with increasing oxidation time. The resistance film, which controls the corrosion mechanism, determined at low frequency increase with increasing oxidation time indication a more resistant oxide against corrosion.

2- The grain size and the surface roughness determined by AFM technique increase with increasing oxidation time t_{ox}. The images obtained by SKPFM show different regions where the corrosion mechanism can be discussed in relation with the variation of the Volta potential.

Acknowledgements

The authors are grateful to the French–Algerian exchange and research program Tassili (Project code CMEP no. 10MDU801) for the financial support of this work.

References

[1] F. Carette, M.C. Lafont, G. Chataignier, L. Guinard, B. Pieraggi, Surf. Interf. Anal. 34 (2002) 135.
[2] M. Da Cunha Belo, N.E. Hakiki, M.G.S. Ferreira, Electrochim. Acta 44 (1999) 2473.
[3] M.G.S. Ferreira, M. Da Cunha Belo, N.E. Hakiki, G. Goodlet, M.F. Montemor, A.M.P. Simoes, J. Braz .Chem. Soc. 13 (2002) 433.
[4] N.E.Hakiki, Corros. Sci., 53 (2011) 2688-2699
[5] N.E.Hakiki, J. Applied Electrochem. 40 (2010) 357-364
[6] N.E.Hakiki, J. Applied Electrochem. 38 (2008) 679-687
[7] B. Maachi, C. Pirri, A. Mehdaoui, N.E. Hakiki, J.L. Bubendorff, Corrosion Science, 53 **(2011)** 984–991
[8] M. Stratmann, Corros. Sci. 27 (1987) 869-872
[9] S.S.El-Egamy, W.A. Badaway, J. Applied Electrochem. 34 (2004) 1153-1158
[10] M.A.Ameer, A.M.Fekry F.El-Taib Heakal , Electrochim. Acta 50 (2004) 43-49
[11] Technical note of the AFM manufacturer (VEECO Society).The used formula is one of the mathematical RMS surface roughnesses.
[12] N. Sathirachinda, R. Petterson, J. Pan, Corros. Sci. (2009) 1850-1860.